Applied Surface Science 479 (2019) 942–952

Contents lists available at ScienceDirect

Applied Surface Science

journal homepage: www.elsevier.com/locate/apsusc

Full length article

Thiolation of polycaprolactone (PCL) nanofibers by inductively coupled plasma (ICP) polymerization: Physical, chemical and biological properties

Mahtab Asadian[a,*], Iuliia Onyshchenko[a], Damien Thiry[b], Pieter Cools[a], Heidi Declercq[c], Rony Snyders[b], Rino Morent[a], Nathalie De Geyter[a]

[a] Research Unit Plasma Technology (RUPT), Department of Applied Physics, Ghent University, Sint-Pietersnieuwstraat 41, B4, B-9000 Ghent, Belgium
[b] Chimie des Interactions Plasma-Surface (ChIPS), CIRMAP, Université de Mons, 20 Place du Parc, B-7000 Mons, Belgium
[c] Tissue Engineering Group, Department of Basic Medical Sciences, Ghent University, De Pintelaan 185, B3, B-9000 Ghent, Belgium

A B S T R A C T

In this study, polycaprolactone (PCL) nanofibrous mats (Ø: 144.2 ± 3.4 nm) were fabricated by electrospinning and subsequently exposed to a low-pressure plasma polymerization treatment using 1-propanethiol as monomer. Surface characterization was performed utilizing several techniques: X-ray photoelectron spectroscopy (XPS) for surface chemical analysis, water contact angle (WCA) measurements for wettability examination, scanning electron microscopy (SEM) for morphological characterization as well as atomic force microscopy (AFM) for visualization of the topography of individual nanofibers before and after the plasma polymerization process. Moreover, the biocompatibility of the untreated and plasma-modified nanofibers was also evaluated by seeding bone marrow stem cells (BMSTs) on the samples and examining cell adhesion and proliferation using live/dead fluorescence imaging and MTT assays. The obtained results revealed that plasma exposure time significantly affected the morphology as well as the surface chemical composition of the electrospun mats, while surface wettability was largely maintained. A short exposure time of 5 s was found to maintain the advantageous nanofibrous morphology as only a very thin coating layer was deposited (range of a few nms), while longer exposure times resulted in a gradual loss of the nanofibrous structure due to the inhomogeneous deposition of thicker coatings. Moreover, also the sulphur amount was found to gradually increase with increasing exposure time resulting from the gradual growth of the deposited thiol-rich coating on the nanofibers with a maximum of 14% of sulphur, correlating with a 6.7% −SH concentration after a plasma polymerization step of 1 min. As the nanofibrous structure is highly advantageous for cell growth, a 5 s plasma exposure time was selected for the cell studies, which proved that the deposition of a very thin thiol-rich coatings was able to positively affect BMSTs adhesion and proliferation. These enhanced cellular responses can be attributed to the presence of thiol groups on the nanofibers which are known to significantly increase the adhesion of culture medium proteins. It can thus be concluded that the incorporation of thiol functionalities via plasma polymerization can positively affect the cellular response of nanofibrous meshes and thus have large potential in tissue engineering applications.

1. Introduction

The application of polymeric nanofibers in the tissue engineering field is strongly increasing due to their morphological similarity to the extracellular matrix (ECM) which is composed of three-dimensional networks of nanoscale fibrous proteins [1]. Tissue engineering is a multidisciplinary science consisting of fundamental principles from materials engineering and biology with the aim to fabricate and develop an alternative substitute for failing tissues and organs [2]. According to literature, the regeneration of damaged tissue is acquired when cells assemble their three-dimensional appearance around and inside a supporting scaffold via biological activities such as adhesion, migration, proliferation, and differentiation [3]. As most human tissues, including bone, cartilage, tendon, skin, nerve, cardiac tissue and blood vessels consist of fibrous structures, with fiber sizes ranging from nanometre to micrometre scale [4–5], artificial nanofibers are considered to be excellent scaffold candidates for tissue engineering applications. The most common nanofiber manufacturing methods are electrospinning [6], phase separation [7] and self–assembly [8]. However, among these methods, electrospinning of polymeric materials has recently received great interest due to its simplicity, versatility, cost-effectivity and scalability [4].

Numerous studies have been performed using various biodegradable synthetic polymeric nanofibers in tissue engineering applications such as polylactic acid (PLA) [9], polyglycolic acid (PGA) [10], poly (lactic-co-glycolic acid) (PLGA) [11], polycaprolactone (PCL) [12–14] or natural ones such as collagen [15], gelatin [16], silk [17] and chitosan [18–19]. However, due to some essential limitations of natural polymers, like weak mechanical properties and poor reproducibility, the usage of synthetic polymers has known a significant boost [20]. Among all synthetic polymers, semi-crystalline linear PCL is one of the most suitable polymers for tissue engineering applications since it is a slowly degradable-FDA-approved polymer – its degradation rate varies between 6 months and 2 years – with excellent mechanical properties

* Corresponding author.
E-mail address: Mahtab.Asadian@UGent.be (M. Asadian).

https://doi.org/10.1016/j.apsusc.2019.02.178

Available online 21 February 2019
0169-4332/

[21]. PCL nanofibers can potentially be used in many applications due to their desirable bulk properties, unfortunately, their surface properties are often not suitable for tissue engineering applications as they exhibit poor cell-material interactions as a result of high surface hydrophobicity [3].

Besides wettability, also the surface chemistry of a nanofibrous scaffold is known to influence cell fate. This factor not only has a direct correlation with surface wettability, but also introduces chemical cues for cell triggering signalling pathways (through protein adsorption), which can control cell growth [22–23]. This biochemical characteristic of nanofibers is an important aspect which can be controlled via surface functionalization of nanofibers. The latter can be achieved through three methods: [1] mixing bioactive agents with the biodegradable polymer solutions to prepare bioactive composite nanofibers during electrospinning [24]; [2] using a coaxial electrospinning technique fabricating core-shell nanofibers [25] or [3] surface modification of nanofibrous scaffolds after electrospinning [26]. Among the above-mentioned methods, nanofiber surface modification is considered as one of the most effective approaches as, under the right conditions, the bulk material properties of the thermoplastic fibrous mat can be preserved. At this moment, a large selection of surface modification strategies is available. Most techniques focus on increasing the wettability through the introduction of a mixture of polar functional groups. Albeit being effective for boosting initial cell adhesion and proliferation, these non-specific modifications tend to be of less interest for tissue engineering, as, in this case, the surface often lacks the proper chemical cues required to interact with the cells' signalling responsible for the metabolic cascade leading to the efficient production of ECM components. In contrast, the introduction of one specific type of functional group at a surface has proven to be very efficient in inducing cell's metabolic pathways required for efficient cell growth and differentiation. Multiple examples are available in literature on the successful incorporation of hydroxy, amines [27], amides [28], carboxylic acids [29], and phosphate groups [30] on solid surfaces and their benign effects on cell surface interactions. Despite the popular use of thiol (-SH) groups for the immobilization of (bio)macromolecules, few studies are available on their cell-interactivity, even though thiols also introduce a strong change in surface wettability, charge and chemical functionality and can have a profound impact on cell-surface interactions [31].

The most commonly used methods employed for thiolation of polymeric materials are wet chemical in nature, for which the substrate is immersed in a solution containing molecules bearing an −SH function [32–33]. For most of these processes, large amounts of solvents, multistep reactions and long reaction times are required to obtain the desired surface, which is unfavourable from an environmental and economical point of view and might be the prime reason for the lack of thiol cell-surface interaction studies, as most alternative types of surface chemistries can be implemented in a more straightforward way [34–39]. Moreover, when attempting to translate these wet chemical treatments onto delicate nanofiber structures, deterioration of their physical and mechanical properties often stands in the way [40]. Finally, (toxic) solvents tend to linger in the chemically-treated nanofibers, thereby negatively affecting their biological response, as solvent residue is known to become trapped into the microporous structure [41]. As such, chemical treatments are not at all preferable for nanofibrous mats intended for biomedical applications, which would explain as to why, to the best of our knowledge, no literature on the thiolation of nanofibers and its effect on cell interactivity is currently available. In this work, we therefore propose the use of non-thermal plasma polymerization of organic monomers containing one or more thiol functionalities as an environmentally friendly and less severe method to generate thiol-rich nanofibers. This technique utilizes a non-thermal plasma discharge to activate the monomer molecules resulting in the deposition of a solid thiol-rich organic layer on a substrate which can be referred to as a plasma polymer film (PPF). In terms of surface engineering, this method offers significant advantages: it is an environmentally friendly, single-step and versatile technique requiring only low reaction times. Furthermore, the deposited layer typically exhibits attractive physico-chemical properties: a good adhesion on most substrates, low solubility in multiple solvents and a high thermal stability. Regarding the formation of thiol-based plasma polymers, Thiry et al. have already examined the influence of process parameters on the physico-chemical properties of thiol-rich PPFs by investigating low-pressure plasma polymerization of 1-propanethiol through the combination of plasma diagnostics methods and PPF analysis [42–45]. From this study, a set of plasma conditions was determined that allowed for the synthesis of 1-propanethiol based PPFs stable in aqueous environments with well-defined chemical compositions on a solid surface [44,46]. In present work, this optimized 1-propanethiol-based coating was deposited, for the first time, on the surface of PCL nanofibers in an effort to generate thiol-rich PCL nanofibers. The plasma-induced changes in surface morphology, topography, wettability and chemical composition of the nanofibers are profoundly investigated. Additional to PPF surface analysis, the surface biological responses of the PCL nanofibers before and after plasma modification are also examined, enabling a correlation between the thiol-rich PPF surface properties and their biological performance.

2. Methods and materials

2.1. PCL nanofiber fabrication

The electrospinning process used to prepare PCL nanofibers has already been optimized and was explained in detail in previous work [13,47]. Briefly, electrospinning was performed on a customized Nanospinner 24 electrospinning machine (Inovenso) at room temperature. First, PCL granules (average molecular weight: 40.000–60.000 $g{\cdot}mol^{-1}$; Sigma-Aldrich) were dissolved in a mixture of formic acid and acetic acid (9:1 v/v) (both from Sigma-Aldrich) to create a 14% w/v PCL solution. Afterwards, this solution was added to a standard syringe, placed in a syringe pump, enabling a PCL solution flow at a rate of 0.7 $ml{\cdot}h^{-1}$ through a tube ending in a metal nozzle. This nozzle was connected to a HV source supplying an applied voltage of 35 kV, while a grounded cylindrical drum placed 15 cm above the nozzle was used as collector. Electrospun PCL fibers were collected on round glass coverslips (Ø = 12 mm) attached to the drum, which was rotating during electrospinning with an angular velocity of 300 rpm.

2.2. Plasma polymerization

In this work, plasma polymerization utilizing 1-propanethiol as precursor (Sigma-Aldrich, 99% purity) was used for PCL nanofiber surface modification. The depositions were carried out in a metallic vacuum chamber pumped by a combination of turbomolecular and primary pumps allowing to reach a residual pressure below 4×10^{-6} Torr. More details about the experimental configuration can be found elsewhere [42]. During the experiments, the working pressure was fixed at 40×10^{-3} Torr and controlled by a throttle valve connected to a capacitive gauge. The plasma was generated using a one-turn inductive water-cooled copper coil (10 cm in diameter) located inside the chamber at a distance of 10 cm in front of the substrate. The coil was connected to an Advanced Energy RF (13.56 MHz) power supply via a matching network. The precursor flow rate and the power were fixed to 10 standard cubic centimetre per minute (sccm) and 100 W respectively. The choice for these experimental parameters was based on previous work [44]: these conditions were found to result in a high stability of the corresponding PPFs in aqueous medium which is essential for the biological tests to be performed in this study [44,48]. As such, in the current work, only the influence of plasma deposition time (from 5 to 60 s) is under investigation.

2.3. Surface characterization of the PCL nanofibers

Scanning electron microscopy (SEM) (JSM-6010 PLUS/LV; JEOL) images were used to examine the morphology of the nanofibers before and after plasma polymerization and were obtained with an accelerating voltage of 7 kV at a working distance of 10 mm. The samples were first coated with a thin layer of gold making use of a sputter coater (JFC-1300 auto fine coater, JEOL) to avoid charge accumulation. The acquired images were also analysed using ImageJ software to determine the diameter distribution of the PCL nanofibers.

The wettability properties of the nanofibers were determined by water contact angle (WCA) measurements using the sessile drop method on a commercial Krüss DSA25 contact angle goniometer. A 2 µl droplet of distilled water was placed on the surface of the nanofibers at room temperature and WCA values were obtained by applying Laplace-Young curve fittings to the imaged water drop profiles. For each treatment condition, 3 different samples were tested on 2 randomly selected positions and a mean contact angle value was determined by averaging all measured WCA values (6 in total).

X-ray photoelectron spectroscopy (XPS) was performed on a PHI Versaprobe II spectrometer. This apparatus was equipped with a monochromatic Al K_α X-ray source ($h\nu$ = 1486.6 eV) and was operated at 25.8 W resulting in a beam diameter of 50 µm. During the measurements, the pressure in the XPS chamber was at least 10^{-6} Pa and the photoelectrons were detected with a hemispherical analyser positioned at an angle of 45° with respect to the normal of the sample surface. Survey scans and individual high-resolution spectra (C1s, O1s and S2p) were recorded with a pass energy of 187.85 eV (0.8 eV step) and 23.5 eV (0.1 eV step) respectively on 5 different locations randomly selected on each PCL sample. Elements present on the surfaces were identified from XPS survey scans and quantified with Multipak (Version 9.6) software using a Shirley background and applying the relative sensitivity factors supplied by the manufacturer of the instrument. CasaXPS software was used to curve fit the high resolution C1s peaks after calibration of the energy scale using the hydrocarbon component of the C1s spectrum (285.0 eV). The C1s peaks were deconvoluted using Gaussian–Lorentzian peak shapes and the full-width at half maximum (FWHM) of each line shape was constrained below 1.5 eV.

Unfortunately, due to restrictions in XPS resolution, even in high resolution XPS spectra specific sulphur-based chemical functional groups cannot be distinguished as individual peaks (e.g., C−SH, C−S−C, C═S, C−S−S) and can thus not be quantified. To overcome this problem, the combination of XPS with chemical derivatization can be employed and has already been widely applied for the quantification of different functional groups [49–50]. Some time ago, Thiry et al. have also used for the first time *N*-ethylmaleimide as labelling molecule for the quantitative determination of −SH functionalities in thiol-rich PPFs synthesized using propanethiol as chemical precursor [46]. This optimized method was also employed in this work: derivatization reactions were carried out in a solution of *N*-ethylmaleimide (99%, Sigma-Aldrich) in phosphate buffer at a concentration of 10^{-1} M for a duration of 86 h. Afterwards, the samples were rinsed in the buffer solution for 5 min to eliminate unreacted molecules and were subsequently dried under a nitrogen flow before starting XPS analysis. The percentage of carbon atoms bearing an -SH group ([SH]) was calculated according to the following equation:

$$[SH](\%) = \frac{[N]}{[C] - 6[N]} \times 100 \quad (1)$$

To determine the roughness of the electrospun PCL nanofibrous samples as well as the roughness of individual PCL nanofibers before and after plasma polymerization, atomic force microscopy (AFM) was utilized. AFM images were obtained with an XE-70 AFM device (Park Scientific Instruments) in non-contact mode using highly doped crystal silicon cantilevers with a spring constant of approximately 40 Nm^{-1}. To acquire comprehensive data from the surface of a single nanofiber, three scanning steps, with the aim to achieve a higher resolution, were followed: first, the nanofibrous mesh was scanned over the largest possible area, after which the area of interest was narrowed down to only one single nanofiber, followed by scanning the surface of the selected nanofiber.

2.4. In vitro cell-material studies

Cell adhesion and proliferation tests were also performed in this work using bone marrow stem cells (BMSTs) as the final objective of this study was to investigate the effects of the performed plasma polymerization step on the cellular response of PCL nanofibers. Before cell seeding, the untreated and plasma-polymerized nanofibrous scaffolds were sterilized by exposure to UV light for 30 min, which was found to be an ideal sterilization method for PCL nanofibers [51–52]. After the sterilization step, the samples were first pre-wetted: they were placed in the wells of a 24-well tissue culture dish (Greiner bio-one) and 0.5 ml culture medium per well was added. After overnight incubation, the culture medium was removed and BMSTs were seeded onto the samples at a density of 6×10^4 cells·ml^{-1} of medium per sample. The used culture medium was DMEM/F-12 (Dulbecco's Modified Eagle Medium/Nutrient Mixture F-12) supplemented with 10% foetal calf serum, 10 µg·ml^{-1} penicillin and 10 mg·ml^{-1} streptomycin (all from Gibco Invitrogen). The cell-seeded samples were maintained in a humidified incubator at 37 °C containing 5% CO_2 for 1 and 7 days and cells were also seeded on tissue culture polystyrene (TCPS) to act as positive control.

To qualitatively evaluate cell viability, a live/dead cell staining was performed 1 day and 7 days post-seeding. Prior to the staining, the supernatant was removed and the samples were rinsed twice with phosphate buffered saline (PBS). Afterwards, the staining was performed by adding 2 µl (1 mg·ml^{-1}) of calcein-acetylmethoxyester (Anaspec) supplemented with 2 µl (1 mg·ml^{-1}) propidium iodide (Sigma-Aldrich) to the cell-seeded samples. Subsequently, the samples were incubated for 10 min at room temperature in the dark, after which they were visualized with a fluorescence microscope (Olympus IX 81) making use of appropriate filters. To obtain more quantitative information, a colorimetric MTT assay, using the yellow tetrazolium dye 3-(4, 5-dimethyldiazol-2-yl)-2, 5-diphenyltetrazolium bromide (MTT, Merck Promega) was also performed in this work to quantify cell viability by colorimetrically measuring the amount of metabolically active BMSTs. In viable cells, the tetrazolium component is reduced by mitochondrial dehydrogenase enzymes into blue-purple water-insoluble formazan, which can be solubilized by adding a lysis buffer and subsequently measured making use of spectrophotometry [53–54]. Cell viability was quantified 1 and 7 days after cell seeding by replacing the culture medium with 0.5 ml (0.5 mg·ml^{-1}) MTT reagent. Subsequently, the samples were incubated at 37 °C in a humidified atmosphere containing 5% CO_2 for 4 h, after which the samples were removed from the MTT reagent and placed in a lysis buffer (1:1 isopropanol/ethanol) to solubilize the water-insoluble formazan. Afterwards, 200 µl of the formazan solution was transferred to a 96-well plate and the absorbance of the coloured solution at 580 nm was measured using a spectrophotometer (Universal microplate reader EL 800, BioTek Instruments). Background absorbance at 750 nm was subtracted from the measured signals and the obtained optical density of the coloured solution was reported as a percentage compared to the TCPS positive control. At day 1 and day 7, the positive control sample of day 1 and day 7 respectively was used. In addition, optical density values were obtained on 3 different samples and will therefore be expressed as mean value ± standard deviation. The obtained data were also used to assess if the differences between samples were significant using one-way ANOVA and multiple comparison tests.

Finally, the morphology of the cells adhering and proliferating on the samples was also visualized by obtaining SEM images of the cell-loaded samples 1 and 7 days after cell seeding. To do so, the

supernatants were first removed from the samples after which the nanofibers were rinsed 3 times with PBS. Afterwards, the cells on the samples were fixed by submerging the samples in a 2.5% glutaraldehyde (Sigma-Aldrich) solution in cacodylate buffer (Sigma-Aldrich) for 1 h at room temperature. Subsequently, the cells were dehydrated by immersing the nanofibers in solutions of ethanol in sterilized water of increasing ethanol concentration (30, 50, 75, 85, 95 and 100%) for 10 min per immersion step. After dehydration, the samples were transferred to a 100% hexamethyldisilazane (HMDS) (Acros organics) solution where they were stored for 10 min. The HMDS solution was subsequently replaced by a fresh HMDS solution, which was left to evaporate under the fume hood. The nanofibrous samples covered with dehydrated, fixed cells were subsequently gold-coated and viewed with SEM at an accelerating voltage and working distance of 7 kV and 10 mm respectively.

3. Results and discussion

3.1. Surface morphology (SEM)

The morphology of electrospun nanofibrous samples is a crucial parameter to examine as it can substantially influence the morphology and growth of seeded cells [4,55–56]. Thus, as a first step, the morphology of PCL nanofibers before and after conducting the plasma polymerization process using different treatment times was examined using SEM. Fig. 1 shows the obtained SEM images for pristine PCL nanofibers (a) and after a plasma polymerization time of 5, 10, 30 and 60 s (b), (c), (d) and (e) respectively. Fig. 1(a) revealed that the untreated PCL sample consisted of randomly oriented smooth PCL nanofibers without the presence of beads resulting in a strongly interconnected, porous nanofibrous mesh. The average fiber diameter was found to be 144.2 ± 3.4 nm, which is significantly smaller than fiber diameters obtained from chloroform-containing PCL solutions, which typically range from 600 nm to several μm [57–58]. The PCL nanofibers obtained in this work thus truly have nano-dimensions and may thus possess unique advantages in tissue engineering applications [59].

After performing the plasma polymerization step with an exposure time of 5 s, the morphology of the nanofibrous sample (Fig. 1(b)) was quite similar to the morphology of the pristine sample. Nevertheless, the PCL fiber diameter was found to be slightly thicker than for the untreated sample (173.8 ± 4.9 nm) suggesting the deposition of a 15 nm thick coating on the PCL nanofibers. By performing a very short plasma polymerization step, it was thus possible to maintain the biomimicking nano-dimensions of the PCL sample. In contrast, significant changes in the nanofibers' morphology were observed upon further increasing the plasma polymerization duration. Starting from 10 s of plasma treatment, the coating assembled on specific areas of the sample resulting in the deposition of non-uniform coatings as can be observed in Fig. 1(c), (d) and (e). Moreover, the original nanofibrous morphology of the samples also gradually disappeared with increasing treatment time as a result of the increased thickness of the polymer coating. In addition, plasma exposure times above 60 s (images not shown here) even resulted in nanofibrous samples completely covered by a solid PPF on top. As the nano-morphology of the samples plays an important role in tissue engineering applications, a fixed plasma polymerization duration of 5 s was chosen for all following experiments.

3.2. Surface wettability (WCA analysis)

To evaluate the wettability of the nanofibers, WCA measurements were performed before and after the 5 s plasma polymerization step. As shown in Table 1, the contact angle of the untreated PCL nanofibers is 140° which reveals the highly hydrophobic characteristics of the pristine PCL sample. This result is in good agreement with WCA values of PCL nanofibers reported before in literature [60–62]. Upon plasma treatment, only a very small decrease in WCA value (137°) was found for the coated PCL nanofibers. This slight decrease in WCA suggests an alternation of the surface chemical properties but could also be attributed to a change in surface roughness after plasma treatment. Indeed, it was already observed that electrospun fibrous mats with different surface morphologies showed different surface roughness values, which in turn resulted in varying volumes of air that is trapped between the interfaces of fibers and water and thus varying WCA values. For example, the surface roughness of electrospun mats was found to increase with decreasing fiber diameters and increasing pore sizes, leading to higher air entrapment in the surface pores and thus larger WCA values [63–64]. To elucidate the effect of surface roughness on the obtained WCA values, additional experiments were conducted and will be described in the following section.

3.3. Surface topography (AFM)

To exactly determine the influence of the plasma polymer layer on the surface topography of the electrospun PCL mats, AFM measurements were conducted, and the results are shown in Fig. 2. Based on the previously depicted SEM image (Fig. 1(b)), it was concluded that due to the plasma polymerization step a thin coating of approximately 15 nm was deposited on individual PCL nanofibers resulting in an electrospun PCL mesh with slightly smaller pore sizes. To obtain more quantitative information on the surface roughness of the electrospun samples, AFM images of a part of the electrospun meshes (45 × 45 μm^2) were also taken (Fig. 2) from which the average and root mean square (RMS) roughness could be determined (Table 2). The obtained results revealed that there was no significant change in the roughness of electrospun PCL mats before and after the plasma polymerization process which is in accordance with the earlier shown SEM images. However, these obtained AFM results do not provide any information on the roughness of a single nanofiber as a large scale area was scanned resulting in an image with lower resolution [65]. Therefore, high resolution AFM images of a single nanofiber were also taken on the untreated and plasma-polymerized samples as nano-scale surface roughness plays an important role in cell-material interactions [66]. Representative AFM images are shown in Fig. 2, while Table 2 provides the average roughness values of different examined samples. Table 2 showed that after plasma polymerization the roughness of the individual PCL fibers increased from 4.6 nm for pristine PCL nanofibers to 8.2 nm for the coated samples (5 s plasma treatment). This increase in fiber surface roughness can be linked to plasma-induced etching effects in combination with film deposition onto the nanofiber surfaces. In fact, the deposition of a plasma-polymerized film relies on a dynamic equilibrium between a process of deposition and a process of chemical ion-assisted etching by incoming active species from the plasma. Electrons, ions, and radicals which are generated in the plasma, bombard the sample surface simultaneously causing etching as well as film deposition resulting into changed surface roughness values [67–69].

As mentioned before, the obtained changes in WCA results for untreated and plasma-polymerized PCL nanofibers could be associated with surface topography. Considering the dimensions of the water droplet used for WCA measurements, mainly the roughness of the electrospun mat instead of the roughness of individual nanofibers need to be taken into account. As this roughness remained unaffected by the plasma polymerization step, it can thus be concluded that the observed minor change in wettability was not due to changes in surface roughness. As such, the different WCA value can thus be fully linked to a different surface chemical composition, which will be further examined in the following section.

3.4. Surface chemical composition (XPS)

In this section, XPS analysis was applied to identify and quantify the surface chemical composition and the surface chemical groups present on the PCL nanofibers before and after plasma polymerization. The

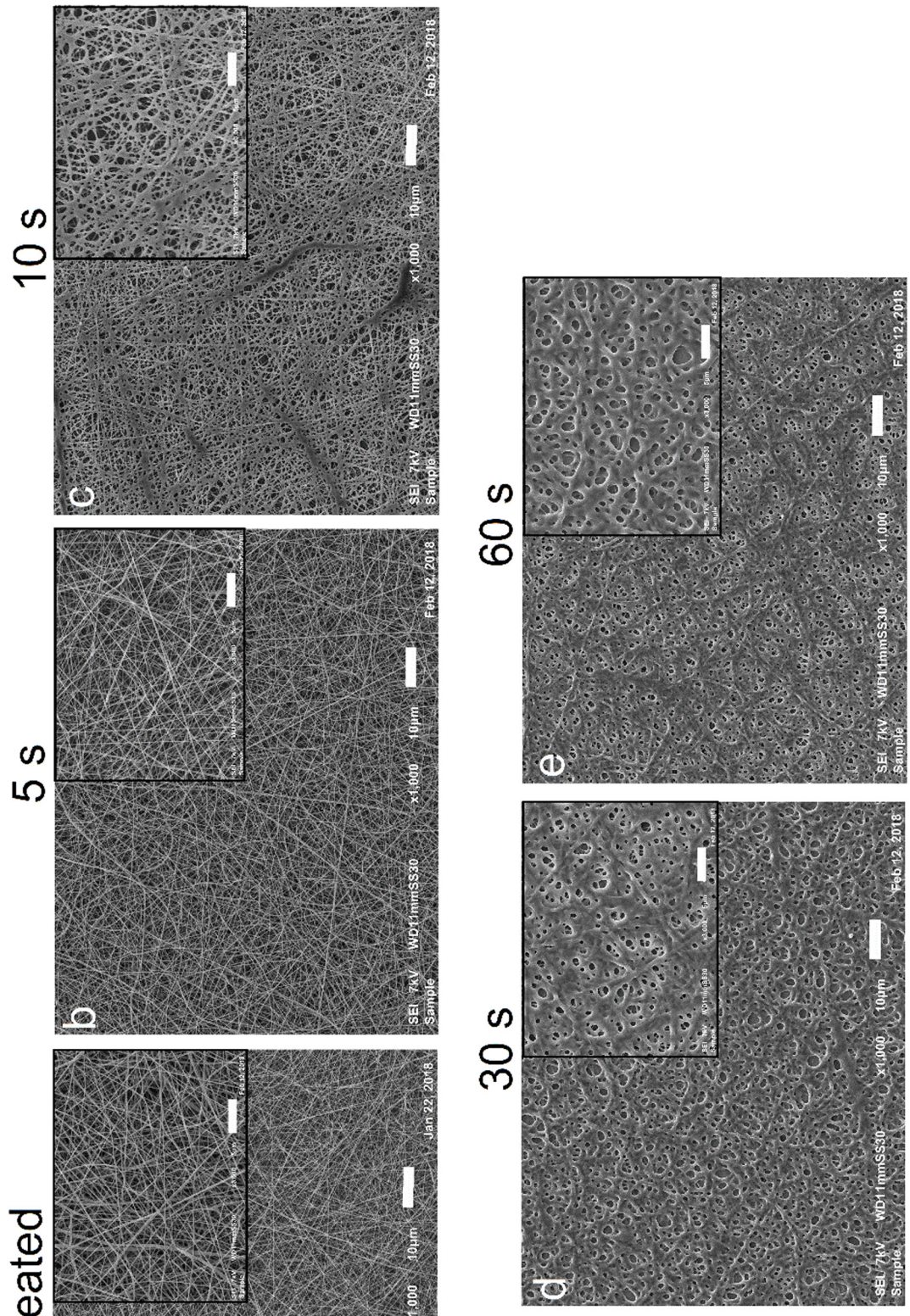

Fig. 1. SEM images of PCL nanofibers before (a) and after plasma polymerization with a plasma exposure time of 5 s (b), 10 s (c), 30 s (d) and 60 s (e) (scale bars = 5 & 10 µm).

Table 1
WCA values and mean fiber diameter for untreated and coated PCL nanofibers.

Sample	WCA (°)	Diameter (nm)
Untreated PCL nanofibers	140.0 ± 1.1	144.2 ± 3.4
Plasma-polymerized PCL nanofibers (5 s)	137.7 ± 0.8	173.8 ± 4.9

Table 2
Surface roughness of untreated and plasma-polymerized electrospun PCL nanofibers. R_a and R_q represent the average and RMS roughness respectively.

Sample	R_q (nm)	R_a (nm)
Untreated electrospun PCL mats	0.6 ± 0.1	0.4 ± 0.1
Plasma-polymerized electrospun PCL mats (5 s)	0.5 ± 0.1	0.4 ± 0.1
Untreated individual PCL nanofibers	4.6 ± 0.2	3.7 ± 0.1
Individual plasma-polymerized PCL nanofibers (5 s)	8.2 ± 1.4	6.4 ± 1.1

results of the elemental surface composition obtained from XPS survey scans are shown in Table 3 revealing that the oxygen concentration for untreated PCL nanofibers is approximately 22% which is slightly lower than the theoretically expected oxygen value for PCL (25%). This difference in oxygen content might be explained by small changes induced during the PCL solution preparation and electrospinning process or more likely due to some polymer contamination. Table 3 also shows that the percentage of detected oxygen on the plasma-modified surfaces was decreasing with polymerization time reaching a minimum value of 15.6% after 60 s plasma treatment. At the same time, the percentage of carbon decreased, while also sulphur was found to be present on the plasma-polymerized samples indicating the successful deposition of a sulphur-containing coating. Table 3 also revealed that the incorporation of sulphur increased within increasing plasma polymerization duration. These differences as a function of treatment time were rather unexpected as surface chemical composition typically remained constant as a function of exposure time when plasma operational parameters were not varied [70]. As such, it could be anticipated that these changes were mainly due to variations in film thickness, which is known to increase with increasing plasma polymerization time [71]. After 5 s, the coating deposited on the nanofibers was so thin that the oxygen peak from the polymer substrate could still be detected in the XPS survey spectra. With increasing plasma exposure time, the coating became thicker and thicker gradually reducing the influence of the PCL substrate thereby resulting in lower oxygen amounts and higher sulphur contents. Moreover, also the inhomogeneous deposition of the coatings at higher exposure times (see Fig. 1) could be responsible for the remaining oxygen peak as some parts of the nanofibers were maybe not nicely covered by the coating. Apart from the above-mentioned reasons, post-oxidation reactions might also be accountable for the oxygen content on the polymerized surfaces. In previous work, the obtained XPS results demonstrated a different surface coating composition [44]: oxygen was not detected in the plasma coating and a higher S/C ratio of approximately 0.40 was found. The different results in this work can be explained by [1] the different substrate (silicon wafer versus PCL nanofibers) and [2] the method of sample preparation. In this work, after the plasma polymerization process, PCL nanofibers were removed from the plasma chamber and were thus exposed to ambient air prior to XPS analysis while in previous work a direct transfer from the plasma to the XPS chamber was performed. As such, post-oxidation reactions can thus occur on the coatings prepared in this work. Moreover, the deposition rate on the flat silicon wafer was previously observed to be slightly less than 25 nm/min suggesting a coating thickness of only 2 nm after a deposition time of 5 s and a coating thickness of 25 nm after 60 s of plasma treatment. However, as the substrates were not flat in this study, but consisted of a 3D structure, it can be anticipated that the final coating thickness on the nanofibers was even smaller considering their significantly higher surface area. From SEM images, however, a higher coating thickness of 15 nm was found after 5 s of plasma polymerization, however, the error on this value can be rather large, taking into account the resolution of the SEM device.

The above-mentioned elemental composition unambiguously indicated the incorporation of sulphur on the PCL nanofibers, but, unfortunately did not provide any information about the retention of the

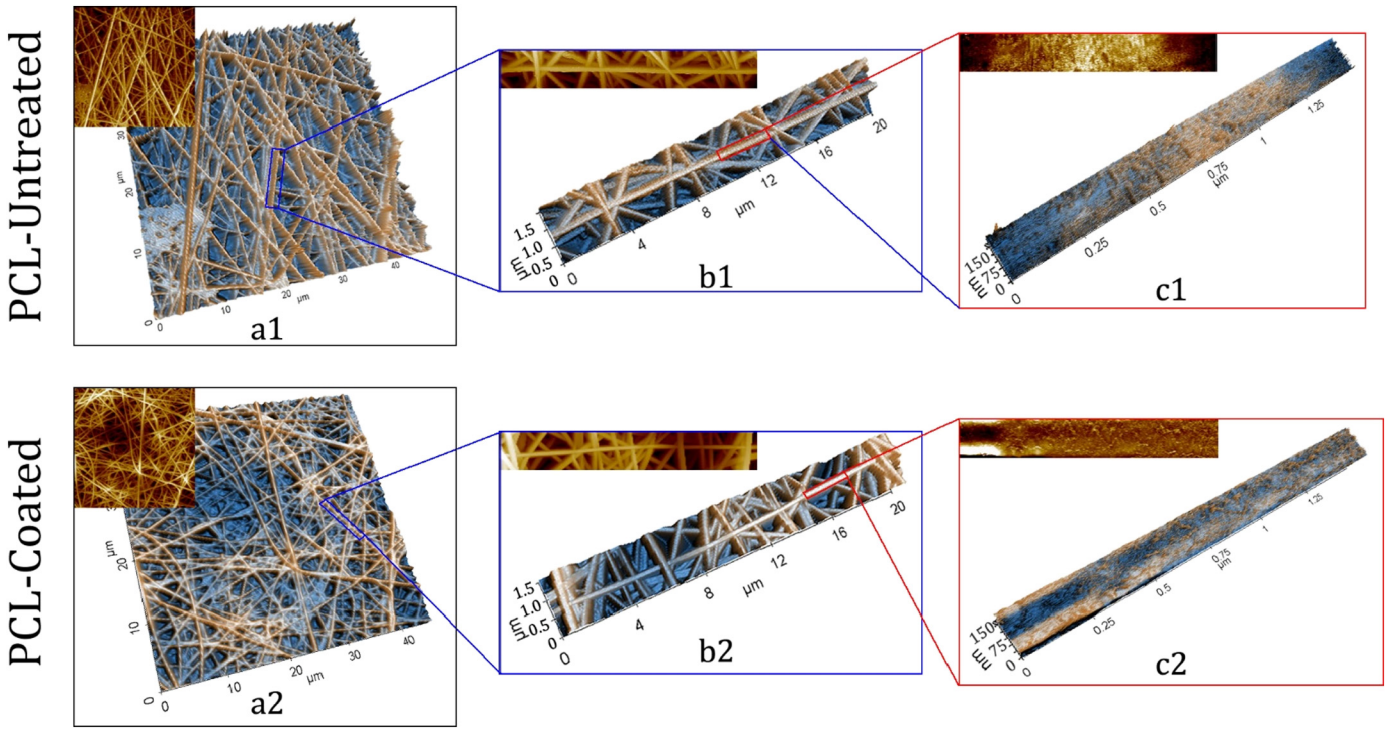

Fig. 2. 3D AFM images of PCL electrospun mats (a), a few nanofibers (b) and the surface of a single nanofiber (c) of untreated and plasma-polymerized samples (5 s exposure time).

Table 3
Chemical composition of untreated and plasma-modified PCL nanofibers before and after chemical derivatization.

	Before derivatization			After derivatization				
	C1s (%)	O1s (%)	S2p (%)	C1s (%)	N1s (%)	O1s (%)	S2p (%)	[SH] (%)
Untreated	78.2 ± 0.6	21.8 ± 0.6	–	75.7 ± 0.5	–	24.3 ± 0.5	–	–
PPF-5 s	73.0 ± 0.7	20.5 ± 0.2	6.5 ± 0.5	72.2 ± 0.1	1.2 ± 0.4	21.1 ± 0.2	5.5 ± 0.4	1.8 ± 0.5
PPF-10 s	70.4 ± 0.0	20.9 ± 0.2	8.7 ± 0.3	69.7 ± 0.9	1.3 ± 0.4	22.5 ± 0.8	6.6 ± 1.3	2.1 ± 0.7
PPF-30 s	71.5 ± 0.4	17.7 ± 0.7	10.8 ± 0.5	72.0 ± 0.3	1.5 ± 0.5	18.0 ± 0.5	8.5 ± 0.4	2.4 ± 0.8
PPF-60 s	70.7 ± 0.1	15.6 ± 0.2	13.7 ± 0.2	67.2 ± 0.9	3.2 ± 0.6	17.9 ± 0.1	11.7 ± 0.8	6.7 ± 0.7

targeted functional group, namely the −SH group. To gather this information, a chemical derivatization step was employed as previously described and the elemental composition of the derivatized samples can be seen in Table 3, together with the calculated percentage of carbon atoms bearing an -SH group ([SH]). After the derivatization procedure, nitrogen, present in the labelling molecule, was clearly identified in the XPS survey spectra as evidenced by the nitrogen amounts presented in Table 3. The results on the derivatized samples additionally demonstrated that with increasing plasma polymerization time, the amount of carbon atoms bearing a thiol group on the PCL nanofibers surface increased from 1.8% to 6.7%, concentrations that are similar to what has been observed for wet-chemical thiolation [38–39]. The increasing amount of surface thiol groups can again be explained by the increasing thickness of the plasma-polymerized coating: at short treatment times, relative less thiol groups were present at the surface due to the significantly large contribution from the PCL substrate.

Additional information regarding the surface functional groups can be obtained by curve fitting the high resolution C1s peaks of the untreated and plasma-polymerized samples. The fitted high resolution C1s peaks are shown in Fig. 3, while Table 4 presents the quantitative results obtained from these spectra. According to literature four different peaks could be used for the curve fitting of PCL nanofibers bearing thiol groups: a peak at 285.0 eV corresponding to hydrocarbon and carbon-carbon bonds (C*−C/C*−H), a peak at 285.5 eV corresponding to a secondary carbon bonded to an ester group (C*−COO) and/or a carbon

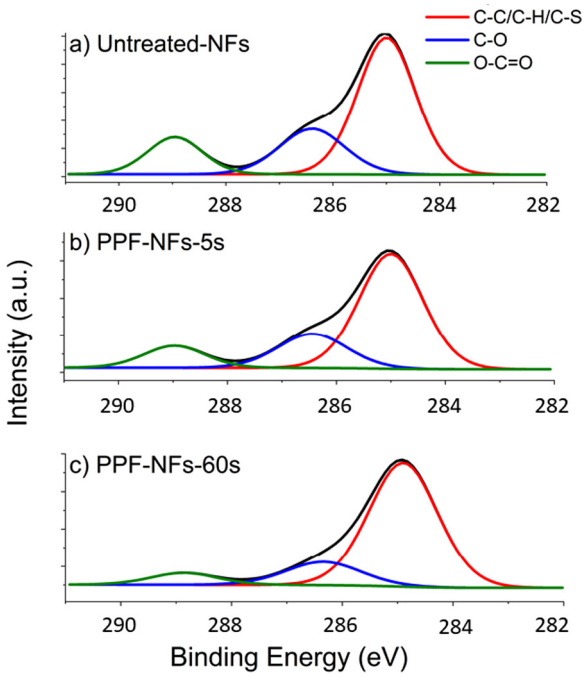

Fig. 3. Deconvolution of the high resolution C1s peaks of (a) untreated PCL nanofibers, plasma-polymerized PCL nanofibers (b) 5 s and (c) 60 s.

Table 4
Relative concentrations of the chemical bonds present on PCL nanofibers as obtained from high resolution C1s deconvolution.

	C1s		
	C−C/C−H/C−S (%) 285.0 eV	C−O (%) 286.4 eV	O−C=O (%) 289.0 eV
Untreated	64.7 ± 0.2	22.1 ± 0.4	13.2 ± 0.5
PPF-PCL-5 s	69.0 ± 0.3	20.0 ± 0.3	11.0 ± 0.4
PPF-PCL-60 s	76.9 ± 0.8	16.0 ± 0.4	7.1 ± 0.5

bonded to sulphur (C*−S), a peak at 286.5 eV corresponding to a carbon single bonded to oxygen (C*−O) and a peak at 289.1 eV corresponding to a carboxyl or ester group (O−C*=O). In this work, however, only three peaks were used for the curve fitting as the limited resolution of the XPS machine made it impossible to make a correct distinction between the peaks located at 285.0 and 285.5 eV. In case of untreated PCL nanofibers, the present chemical bonds were thus C−C/C−H (at 285.0 eV), C−O (at 286.4 eV) and O−C=O (at 289.0 eV), while in case of the plasma-treated samples the peak at 285.0 eV could be attributed to both C−C/C−H as well as C−S bonds. Both Fig. 3 and Table 4 confirmed the incorporation of new sulphur functionalities on the PCL nanofiber surfaces since the peak area and thus also the relative concentration of the C−C/C−H/C−S peak at 285.0 eV increased for the plasma-polymerized samples. Simultaneously, the relative concentration of the peaks at 286.4 and 289.0 eV attributed to C−O and O−C=O groups decreased after the plasma polymerization step, which agrees with the decrease in total oxygen content as shown in Table 3. The decrease in these functional groups, which are only present on the PCL nanofibrous substrates, can be explained by the gradual covering of the substrate with the sulphur-rich coating. Indeed, when the plasma exposure time was increased to 60 s, the relative concentration of these oxygen groups was found to further decrease, while the peak at 285.0 eV increased because of the increasing amount of C−S functional groups.

3.5. Cell-material interactions and cell morphology

After examining the surface physical and chemical characteristics of the untreated and plasma-modified nanofibrous meshes in the previous sections, the impact of the performed plasma polymerization step on the cellular interactions of the PCL meshes were examined in detail in the final part of this work. According to Liu et al., only a small amount of thiol surface groups can improve the biocompatibility of a material and even control adipose stem cell differentiation [31]. Considering this conclusion as well as earlier demonstrated results regarding surface morphology, the 5 s treatment time was chosen to be the optimum condition for these biological tests.

In this section particularly, the morphology of the BMSTs cultured on both untreated and plasma-coated PCL nanofibers was examined by SEM and fluorescence microscopy 1 and 7 days after cell seeding and the results are presented in Fig. 4. On the untreated PCL nanofibers, a

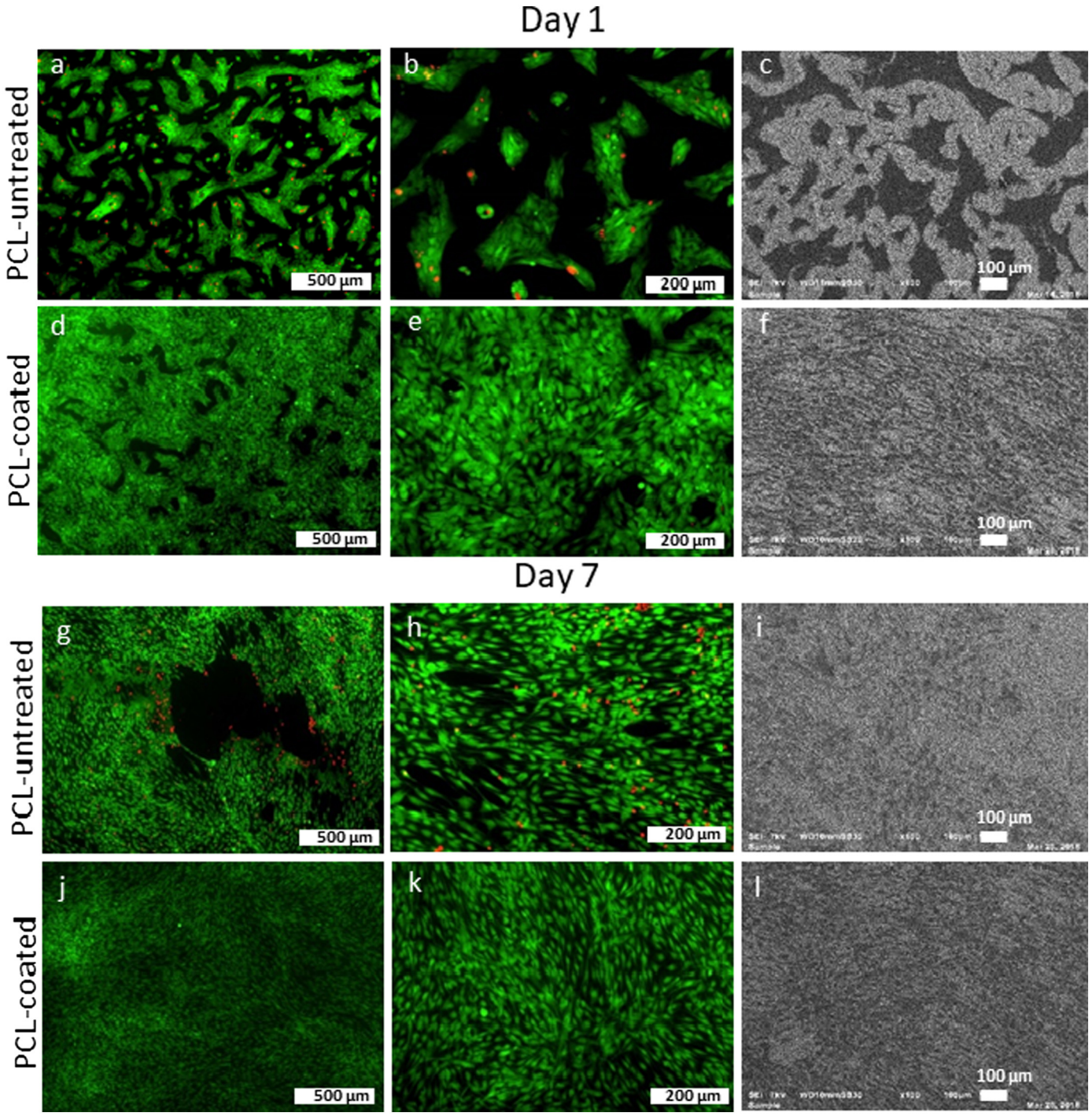

Fig. 4. Fluorescent micrographs after live/dead staining and SEM images of BMSTs seeded on untreated and plasma-polymerized PCL nanofibers 1 day and 7 days after cell seeding.

considerable amount of BMSTs adhered, however, the adherence of these cells was highly inhomogeneous showing regions with a high number of adhered cells as well as regions with no cells (Fig. 4(a), (b) and (c)). Moreover, some red spots due to dead cells were also observed indicating limited cell attachment to the surface of the untreated nanofibers. In contrast, the thiol-coated PCL nanofibers showed numerous attached cells which were almost homogeneously spread over the surface, similar to the appearance of cells growing on TCPS (Fig. 4(d), (e), and (f)). On the plasma-modified nanofibrous meshes, the viable cells were homogeneously flattened and elongated with a significantly higher cell density compared to the untreated sample demonstrating an excellent initial cell adhesion.

Fluorescent and SEM imaging were also performed 7 days after culturing to investigate cell proliferation (Fig. 4(g)–(l)). Fig. 4 showed the presence of a small number of red spots (dead cells) on the untreated sample (Fig. 4(g) and (h)), which were not seen on the plasma-polymerized sample giving a first indication of the lower cell-surface affinity of the untreated sample. Moreover, 7 days after cell seeding, the plasma polymer coated samples were fully covered with cells, whereas some cell-free spots on the surface of the untreated samples were still present. SEM images (Fig. 4(i) and (l)) also showed an almost similar cell morphology on both samples under study: all cells were elongated

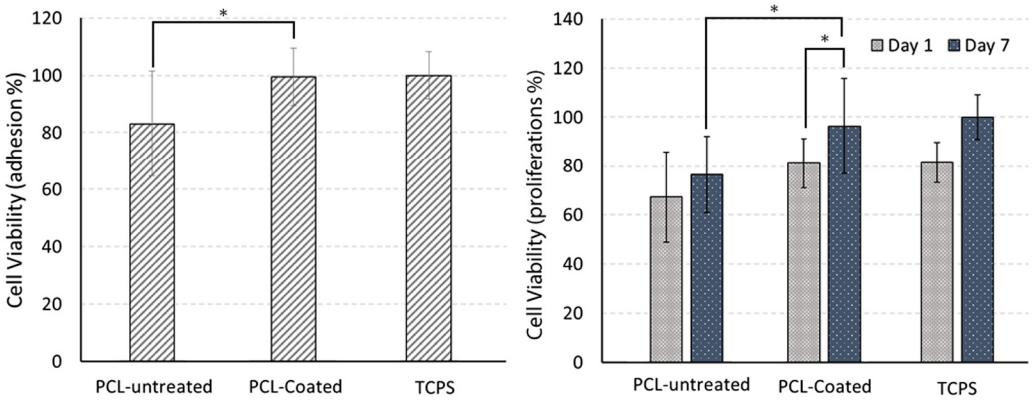

Fig. 5. Percentage of viable BMSTs compared to TCPS 1 day and 7 days after culturing on untreated and plasma-polymerized PCL nanofibers (left: cell adhesion, right: cell proliferation).

and well spread after 7 days. This alike behaviour can be explained by the favourable 3D structure of both samples providing multiple anchoring points for cells.

As the images shown above only provide qualitative information on cellular response, an MTT assay was also performed to quantify cell viability and the obtained results, relative to TCPS, are shown in Fig. 5. 1 day after cell seeding (Fig. 5, left graph), cell viability was found to be higher on the plasma-polymerized sample, showing a similar cell viability as obtained on TCPS. These results are thus in good agreement with the previously shown fluorescence images. Cell viability results also revealed the already good cell adhesion (80% compared to TCPS) on pristine PCL nanofibers, which is in agreement with studies published before and which can be attributed to the 3D nanofibrous structure [14,72–73]. Cell viability was also determined 7 days after cell seeding of which the results are presented in Fig. 5 (left graph). The percentage of viable BMSTs proliferating on thiol-coated PCL nanofibers was significantly higher compared to the untreated sample, showing the positive influence of the thiol-containing coating on cell proliferation.

The enhanced cellular adhesion and proliferation can be attributed to the plasma polymerization process, which affects both the surface chemistry of the PCL nanofibers as well as the topography of the individual PCL nanofibers. The slightly increased roughness of nanofibers after plasma polymerization can positively affect cell growth as surface nano-roughness is known to improve cell adhesion as well as cell proliferation [74–75]. More importantly, the improved adhesion and proliferation can also be linked to the incorporation of thiol groups on the PCL samples. Indeed, previous studies have already indicated that the presence of thiol groups on glass substrates can significantly increase laminin and fibronectin adsorption, which in turn was found to improve fibroblast adhesion [76–77]. Based on these findings, the larger number of adherent cells on thiol-rich surfaces in this study might thus be explained by a higher concentration of adsorbed specific cell binding proteins (such as fibronectin and laminin) which are present in the media culture. In case of pristine PCL nanofibers, the surface lacks suitable bioactive sites for the adsorption of these proteins resulting in less favourable conditions for cell adhesion and proliferation. It can thus be concluded that the deposition of a very thin thiol-containing coating is capable of enhancing cellular interaction on PCL nanofibers without affecting the advantageous nanofibrous morphology of the electrospun PCL samples.

4. Conclusion

In this work, the surface properties of electrospun PCL nanofibers were modified using a low-pressure plasma polymerization process from 1-propanethiol at different treatment times (ranging from 5 s to 60 s). According to SEM and AFM results, a 5 s plasma exposure did not cause significant morphological and topographical changes to the PCL nanofibrous samples as in this case only a very thin (order of nanometres) coating was deposited on the PCL nanofibers. However, the topography of an individual PCL nanofiber was found to possess a slightly increased surface roughness. In contrast, longer treatment times induced noticeable changes that led to the loss of the advantageous nanostructure of the untreated electrospun mat. As such, a plasma exposure time of 5 s was use for further analysis. XPS results also proved the incorporation of sulphur-containing functional groups on the PCL polymer surface, while XPS chemical derivatization also evidenced the incorporation between 1.8 and 6.7% of -SH groups on the plasma-polymerized samples depending on the deposition time. The signal from the oxygen-containing groups, present on the pristine PCL sample, decreased after plasma polymerization as the nanofibers were gradually covered by a thin thiol-rich coating containing no oxygen. This observation again evidenced the low coating thickness at short plasma exposure times. The induced surface chemical changes were also found to positively affect cellular interactions as they caused an improvement in BMST cell adhesion and proliferation because of the plasma polymerization process. As a concluding remark, it can be stated that thiol-rich PCL nanofibers can be considered as potential candidates for a variety of tissue engineering applications due to their strongly promoted cell-surface interactions.

Acknowledgements

This research study has received funding from the European Research Council (ERC) under the European Union's Seventh Framework Program (FP/2007-2013)/ERC Grant Agreement 335929 (PLASMATS) and was also supported by a research grant (G038015N) from the Research Foundation Flanders (FWO). D. Thiry thanks the Région Wallone through the CLEANAIR project for financial support.

References

[1] Z. Ma, M. Kotaki, R. Inai, S. Ramakrishna, Potential of nanofiber matrix as tissue-engineering scaffolds, Tissue Eng. 11 (1–2) (2005) 101–109.
[2] I.-Y. Kim, S.-J. Seo, H.-S. Moon, M.-K. Yoo, I.-Y. Park, B.-C. Kim, C.-S. Cho, Chitosan and its derivatives for tissue engineering applications, Biotechnol. Adv. 26 (1) (2008) 1–21.
[3] Y. Zhang, J. Venugopal, Z.-M. Huang, C. Lim, S. Ramakrishna, Characterization of the surface biocompatibility of the electrospun PCL-collagen nanofibers using fibroblasts, Biomacromolecules 6 (5) (2005) 2583–2589.
[4] C.P. Barnes, S.A. Sell, E.D. Boland, D.G. Simpson, G.L. Bowlin, Nanofiber technology: designing the next generation of tissue engineering scaffolds, Adv. Drug Deliv. Rev. 59 (14) (2007) 1413–1433.
[5] Kadler, K. E.; Holmes, D. F.; Trotter, J. A.; Chapman, J. A., Collagen fibril formation. Biochem. J. 1996, 316 (Pt 1), 1.
[6] J.D. Schiffman, C.L. Schauer, A review: electrospinning of biopolymer nanofibers and their applications, Polym. Rev. 48 (2) (2008) 317–352.
[7] G. Li, P. Li, C. Zhang, Y. Yu, H. Liu, S. Zhang, X. Jia, X. Yang, Z. Xue, S. Ryu,

Inhomogeneous toughening of carbon fiber/epoxy composite using electrospun polysulfone nanofibrous membranes by in situ phase separation, Compos. Sci. Technol. 68 (3–4) (2008) 987–994.
[8] M. Rolandi, R. Rolandi, Self-assembled chitin nanofibers and applications, Adv. Colloid Interf. Sci. 207 (2014) 216–222.
[9] V.C.-H. Tseng, C.H. Chew, W.-T. Huang, Y.-K. Wang, K.-S. Chen, S.-Y. Chou, C.-C. Chen, An effective cell coculture platform based on the electrospun microtube array membrane for nerve regeneration, Cells Tissues Organs 250 (2017) 179–190.
[10] E.D. Boland, T.A. Telemeco, D.G. Simpson, G.E. Wnek, G.L. Bowlin, Utilizing acid pretreatment and electrospinning to improve biocompatibility of poly (glycolic acid) for tissue engineering, J. Biomed. Mater. Res. B Appl. Biomater. 71 (1) (2004) 144–152.
[11] D.A. Stout, B. Basu, T.J. Webster, Poly (lactic–co-glycolic acid): carbon nanofiber composites for myocardial tissue engineering applications, Acta Biomater. 7 (8) (2011) 3101–3112.
[12] F. Chen, C.N. Lee, S.H. Teoh, Nanofibrous modification on ultra-thin poly(e-caprolactone) membrane via electrospinning, Mater. Sci. Eng. C 27 (2007) 325–332.
[13] M. Asadian, M. Dhaenens, I. Onyshchenko, S. De Waele, H. Declercq, P. Cools, B. Devreese, D. Deforce, R. Morent, N. De Geyter, Plasma functionalization of polycaprolactone nanofibers changes protein interactions with cells, resulting in increased cell viability, ACS Appl. Mater. Interfaces 10 (49) (2018) 41962–41977.
[14] M. Asadian, A. Rashidi, M. Majidi, M. Mehrjoo, B.A. Emami, H. Tavassoli, M.P. Asl, S. Bonakdar, Nanofiber protein adsorption affected by electrospinning physical processing parameters, J. Iran. Chem. Soc. 12 (6) (2015) 1089–1097.
[15] W. He, T. Yong, W.E. Teo, Z. Ma, S. Ramakrishna, Fabrication and endothelialization of collagen-blended biodegradable polymer nanofibers: potential vascular graft for blood vessel tissue engineering, Tissue Eng. 11 (9–10) (2005) 1574–1588.
[16] X. Liu, L.A. Smith, J. Hu, P.X. Ma, Biomimetic nanofibrous gelatin/apatite composite scaffolds for bone tissue engineering, Biomaterials 30 (12) (2009) 2252–2258.
[17] M. Rajabi, M. Firouzi, Z. Hassannejad, I. Haririan, P. Zahedi, Fabrication and characterization of electrospun laminin-functionalized silk fibroin/poly(ethylene oxide) nanofibrous scaffolds for peripheral nerve regeneration, J. Biomed. Mater. Res. B Appl. Biomater. (2017) 1–10.
[18] M.E. Frohbergh, A. Katsman, G.P. Botta, P. Lazarovici, C.L. Schauer, U.G. Wegst, P.I. Lelkes, Electrospun hydroxyapatite-containing chitosan nanofibers crosslinked with genipin for bone tissue engineering, Biomaterials 33 (36) (2012) 9167–9178.
[19] M. Asadian, I. Onyshchenko, M. Thukkaram, P.S.E. Tabaei, J. Van Guyse, P. Cools, H. Declercq, R. Hoogenboom, R. Morent, N. De Geyter, Effects of a dielectric barrier discharge (DBD) treatment on chitosan/polyethylene oxide nanofibers and their cellular interactions, Carbohydr. Polym. 201 (2018) 402–415.
[20] M. Norouzi, S.M. Boroujeni, N. Omidvarkordshouli, M. Soleimani, Advances in skin regeneration: application of electrospun scaffolds, Advanced healthcare materials 4 (8) (2015) 1114–1133.
[21] M. Abedalwafa, F. Wang, L. Wang, C. Li, Biodegradable poly-epsilon-caprolactone (PCL) for tissue engineering applications: a review, Rev. Adv. Mater. Sci. 34 (2) (2013) 123–140.
[22] D. Grafahrend, K.-H. Heffels, M.V. Beer, P. Gasteier, M. Möller, G. Boehm, P.D. Dalton, J. Groll, Degradable polyester scaffolds with controlled surface chemistry combining minimal protein adsorption with specific bioactivation, Nat. Mater. 10 (1) (2011) 67–73.
[23] V. Serpooshan, M. Mahmoudi, M. Zhao, K. Wei, S. Sivanesan, K. Motamedchaboki, A.V. Malkovskiy, A.B. Goldstone, J.E. Cohen, P.C. Yang, Protein corona influences cell–biomaterial interactions in nanostructured tissue engineering scaffolds, Adv. Funct. Mater. 25 (28) (2015) 4379–4389.
[24] M.P. Prabhakaran, D. Kai, L. Ghasemi-mobarakeh, Surface modified electrospun nanofibrous scaffolds for nerve tissue engineering, Nanotechnology 19 (45) (2008) 1–8.
[25] Y. Zhang, Z.-M. Huang, X. Xu, C.T. Lim, S. Ramakrishna, Preparation of core − shell structured PCL-r-gelatin bi-component nanofibers by coaxial electrospinning, Chem. Mater. 16 (18) (2004) 3406–3409.
[26] D. Yan, J. Jones, X. Yuan, X. Xu, J. Sheng, J.M. Lee, G. Ma, Q. Yu, Plasma treatment of electrospun PCL random nanofiber meshes (NFMs) for biological property improvement, J. Biomed. Mater. Res. A 101 (4) (2013) 963–972.
[27] H. Park, K.Y. Lee, S.J. Lee, K.E. Park, W.H. Park, Plasma-treated poly (lactic-co-glycolic acid) nanofibers for tissue engineering, Macromol. Res. 15 (3) (2007) 238–243.
[28] D. Sankar, K. Shalumon, K. Chennazhi, D. Menon, R. Jayakumar, Surface plasma treatment of poly (caprolactone) micro, nano, and multiscale fibrous scaffolds for enhanced osteoconductivity, Tissue Eng. A 20 (11 − 12) (2014) 1689–1702.
[29] Z. Ma, W. He, T. Yong, S. Ramakrishna, Grafting of gelatin on electrospun poly (caprolactone) nanofibers to improve endothelial cell spreading and proliferation and to control cell orientation, Tissue Eng. 11 (7–8) (2005) 1149–1158.
[30] G.D. Stynes, T.R. Gengenbach, G.K. Kiroff, W.A. Morrison, M.A. Kirkland, Thiol surface functionalization via continuous phase plasma polymerization of allyl mercaptan, with subsequent maleimide-linked conjugation of collagen, J. Biomed. Mater. Res. A 105 (7) (2017) 1940–1948.
[31] X. Liu, J. He, S. Zhang, X.M. Wang, H.Y. Liu, F.Z. Cui, Adipose stem cells controlled by surface chemistry, J. Tissue Eng. Regen. Med. 7 (2) (2013) 112–117.
[32] S. Li, X. Yue, Y. Jing, S. Bai, Z. Dai, Fabrication of zonal thiol-functionalized silica nanofibers for removal of heavy metal ions from wastewater, Colloids Surf. A Physicochem. Eng. Asp. 380 (1–3) (2011) 229–233.
[33] J. Wang, H.-B. Yao, D. He, C.-L. Zhang, S.-H. Yu, Facile fabrication of gold nanoparticles-poly (vinyl alcohol) electrospun water-stable nanofibrous mats: efficient substrate materials for biosensors, ACS Appl. Mater. Interfaces 4 (4) (2012) 1963–1971.
[34] A. Bernkop-Schnürch, M. Hornof, T. Zoidl, Thiolated polymers—thiomers: synthesis and in vitro evaluation of chitosan–2-iminothiolane conjugates, Int. J. Pharm. 260 (2) (2003) 229–237.
[35] R. Sharma, M. Ahuja, Thiolated pectin: synthesis, characterization and evaluation as a mucoadhesive polymer, Carbohydr. Polym. 85 (3) (2011) 658–663.
[36] Y.-T. Kim, T. Mitani, Surface thiolation of carbon nanotubes as supports: a promising route for the high dispersion of Pt nanoparticles for electrocatalysts, J. Catal. 238 (2) (2006) 394–401.
[37] L.D. Unsworth, Z. Tun, H. Sheardown, J.L. Brash, Chemisorption of thiolated poly (ethylene oxide) to gold: surface chain densities measured by ellipsometry and neutron reflectometry, J. Colloid Interface Sci. 281 (1) (2005) 112–121.
[38] R. Yang, Y. Su, K.B. Aubrecht, X. Wang, H. Ma, R.B. Grubbs, B.S. Hsiao, B. Chu, Thiol-functionalized chitin nanofibers for As (III) adsorption, Polymer 60 (2015) 9–17.
[39] L.-W. Feng, F.-Q. Li, Z.-M. Zhang, L. Yan, Preparation of thiolation poly (aryl ether ketone) nanofiber mat and its adsorption of Hg 2+ ions, Russ. J. Appl. Chem. 89 (10) (2016) 1706–1712.
[40] H.S. Yoo, T.G. Kim, T.G. Park, Surface-functionalized electrospun nanofibers for tissue engineering and drug delivery, Adv. Drug Deliv. Rev. 61 (12) (2009) 1033–1042.
[41] J. Xie, X. Li, Y. Xia, Putting electrospun nanofibers to work for biomedical research, Macromol. Rapid Commun. 29 (22) (2008) 1775–1792.
[42] D. Thiry, N. Britun, S. Konstantinidis, J.-P. Dauchot, M. Guillaume, J.r.m. Cornil, R. Snyders, Experimental and theoretical study of the effect of the inductive-to-capacitive transition in propanethiol plasma polymer chemistry, J. Phys. Chem. C 117 (19) (2013) 9843–9851.
[43] D. Thiry, F.J. Aparicio, N. Britun, R. Snyders, Concomitant effects of the substrate temperature and the plasma chemistry on the chemical properties of propanethiol plasma polymer prepared by ICP discharges, Surf. Coat. Technol. 241 (2014) 2–7.
[44] D. Thiry, R. Francq, D. Cossement, M. Guillaume, J. Cornil, R. Snyders, A detailed description of the chemistry of thiol supporting plasma polymer films, Plasma Process. Polym. 11 (6) (2014) 606–615.
[45] F.J. Aparicio, D. Thiry, P. Laha, R. Snyders, Wide range control of the chemical composition and optical properties of propanethiol plasma polymer films by regulating the deposition temperature, Plasma Process. Polym. 13 (8) (2016) 814–822.
[46] D. Thiry, R. Francq, D. Cossement, D. Guerin, D. Vuillaume, R. Snyders, Establishment of a derivatization method to quantify thiol function in sulfur-containing plasma polymer films, Langmuir 29 (43) (2013) 13183–13189.
[47] Asadian, M.; Dhaenens, M.; Onyshchenko, I.; De Waele, S.; Cools, P.; Devreese, B.; Deforce, D.; Morent, R.; De Geyter, N., Plasma functionalization of PCL nanofibers changes protein interactions with cells resulting in increased cell viability. ACS Applied Materials & Interfaces 2018, submitted.
[48] L. Detomaso, R. Gristina, G.S. Senesi, R. d'Agostino, P. Favia, Stable plasma-deposited acrylic acid surfaces for cell culture applications, Biomaterials 26 (18) (2005) 3831–3841.
[49] G. Aziz, N. De Geyter, R. Morent, Incorporation of primary amines via plasma technology on biomaterials, Advances in Bioengineering, Intech, 2015, pp. 21–47.
[50] P. Hamerli, T. Weigel, T. Groth, D. Paul, Surface properties of and cell adhesion onto allylamine-plasma-coated polyethylenterephtalat membranes, Biomaterials 24 (22) (2003) 3989–3999.
[51] N.A. Trujillo, K.C. Popat, Increased adipogenic and decreased chondrogenic differentiation of adipose derived stem cells on nanowire surfaces, Materials 7 (4) (2014) 2605–2630.
[52] R. Ghobeira, C. Philips, H. Declercq, P. Cools, N. De Geyter, R. Cornelissen, R. Morent, Effects of different sterilization methods on the physico-chemical and bioresponsive properties of plasma-treated polycaprolactone films, Biomed. Mater. 12 (1) (2017) 015017.
[53] J.C. Stockert, A. Blázquez-Castro, M. Cañete, R.W. Horobin, Á. Villanueva, MTT assay for cell viability: intracellular localization of the formazan product is in lipid droplets, Acta Histochem. 114 (8) (2012) 785–796.
[54] G. Ciapetti, E. Cenni, L. Pratelli, A. Pizzoferrato, In vitro evaluation of cell/biomaterial interaction by MTT assay, Biomaterials 14 (5) (1993) 359–364.
[55] J. Shi, A.R. Votruba, O.C. Farokhzad, R. Langer, Nanotechnology in drug delivery and tissue engineering: from discovery to applications, Nano Lett. 10 (9) (2010) 3223–3230.
[56] S.J. Hollister, Porous scaffold design for tissue engineering, Nat. Mater. 4 (7) (2005) 518–524.
[57] O. Hartman, C. Zhang, E.L. Adams, M.C. Farach-Carson, N.J. Petrelli, B.D. Chase, J.F. Rabolt, Biofunctionalization of electrospun PCL-based scaffolds with perlecan domain IV peptide to create a 3-D pharmacokinetic cancer model, Biomaterials 31 (21) (2010) 5700–5718.
[58] J.L. Lowery, N. Datta, G.C. Rutledge, Effect of fiber diameter, pore size and seeding method on growth of human dermal fibroblasts in electrospun poly (ε-caprolactone) fibrous mats, Biomaterials 31 (3) (2010) 491–504.
[59] T.J. Sill, H.A. von Recum, Electrospinning: applications in drug delivery and tissue engineering, Biomaterials 29 (13) (2008) 1989–2006.
[60] R. Ghobeira, C. Philips, V. De Naeyer, H. Declercq, P. Cools, N. De Geyter, R. Cornelissen, R. Morent, Comparative study of the surface properties and cytocompatibility of plasma-treated poly-ε-caprolactone nanofibers subjected to different sterilization methods, J. Biomed. Nanotechnol. 13 (6) (2017) 699–716.
[61] D. Kai, M.P. Prabhakaran, G. Jin, S. Ramakrishna, Guided orientation of cardiomyocytes on electrospun aligned nanofibers for cardiac tissue engineering, J. Biomed. Mater. Res. B Appl. Biomater. 98 (2) (2011) 379–386.
[62] A. Martins, E.D. Pinho, S. Faria, I. Pashkuleva, A.P. Marques, R.L. Reis, N.M. Neves, Surface modification of electrospun polycaprolactone nanofiber meshes by plasma treatment to enhance biological performance, small 5 (10) (2009) 1195–1206.

[63] W. Cui, X. Li, S. Zhou, J. Weng, Degradation patterns and surface wettability of electrospun fibrous mats, Polym. Degrad. Stab. 93 (3) (2008) 731–738.
[64] H. Wu, R. Zhang, Y. Sun, D. Lin, Z. Sun, W. Pan, P. Downs, Biomimetic nanofiber patterns with controlled wettability, Soft Matter 4 (12) (2008) 2429–2433.
[65] K.D. Jandt, Atomic force microscopy of biomaterials surfaces and interfaces, Surf. Sci. 491 (3) (2001) 303–332.
[66] S.P. Khan, G.G. Auner, G.M. Newaz, Influence of nanoscale surface roughness on neural cell attachment on silicon, Nanomedicine 1 (2) (2005) 125–129.
[67] G. Aziz, M. Thukkaram, N. De Geyter, R. Morent, Plasma parameters effects on the properties, aging and stability behaviors of allylamine plasma coated ultra-high molecular weight polyethylene (UHMWPE) films, Appl. Surf. Sci. 409 (2017) 381–395.
[68] A. Manakhov, M. Landová, Cyclopropylamine plasma polymers for increased cell adhesion and growth, Plasma Process. Polym. 14 (7) (2016) 1–12.
[69] A. Choukourov, H. Biederman, D. Slavinska, L. Hanley, A. Grinevich, H. Boldyryeva, A. Mackova, Mechanistic studies of plasma polymerization of allylamine, J. Phys. Chem. B 109 (48) (2005) 23086–23095.
[70] K.V. Chan, I. Onyshchenko, A. Nikiforov, G. Aziz, R. Morent, N. De Geyter, Plasma polymerization of cyclopropylamine with a sub-atmospheric pressure DBD, Eur. Polym. J. 103 (2018) 1–10.
[71] R. Morent, N. De Geyter, T. Jacobs, S. Van Vlierberghe, P. Dubruel, C. Leys, E. Schacht, Plasma-polymerization of HMDSO using an atmospheric pressure dielectric barrier discharge, Plasma Process. Polym. 6 (S1) (2009) S537–S542.
[72] Kweon, H.; Yoo, M. K.; Park, I. K.; Kim, T. H.; Lee, H. C.; Lee, H.-S.; Oh, J.-S.; Akaike, T.; Cho, C.-S., A novel degradable polycaprolactone networks for tissue engineering. Biomaterials 2003, 24 (5), 801–808.
[73] Khil, M. S.; Bhattarai, S. R.; Kim, H. Y.; Kim, S. Z.; Lee, K. H., Novel fabricated matrix via electrospinning for tissue engineering. Journal of Biomedical Materials Research Part B: Applied Biomaterials: An Official Journal of The Society for Biomaterials, The Japanese Society for Biomaterials, and The Australian Society for Biomaterials and the Korean Society for Biomaterials 2005, 72 (1), 117–124.
[74] N.J. Hallab, K.J. Bundy, K. O'Connor, R.L. Moses, J.J. Jacobs, Evaluation of metallic and polymeric biomaterial surface energy and surface roughness characteristics for directed cell adhesion, Tissue Eng. 7 (1) (2001) 55–71.
[75] F. Zamani, M. Amani-Tehran, M. Latifi, M.A. Shokrgozar, The influence of surface nanoroughness of electrospun PLGA nanofibrous scaffold on nerve cell adhesion and proliferation, J. Mater. Sci. Mater. Med. 24 (6) (2013) 1551–1560.
[76] K. Webb, V. Hlady, P.A. Tresco, Relative importance of surface wettability and charged functional groups on NIH 3T3 fibroblast attachment, spreading, and cytoskeletal organization, J. Biomed. Mater. Res. 41 (3) (1998) 422.
[77] Webb, K.; Hlady, V.; Tresco, P. A., Relationships among cell attachment, spreading, cytoskeletal organization, and migration rate for anchorage-dependent cells on model surfaces. Journal of Biomedical Materials Research: An Official Journal of The Society for Biomaterials and The Japanese Society for Biomaterials 2000, 49 (3), 362–368.